

## Supporting Information

Understanding selectivity for the electrochemical reduction of carbon dioxide to formic acid and carbon monoxide on metal electrodes

Jeremy T. Feaster<sup>1,2</sup>, Chuan Shi<sup>1,2</sup>, Etosha R. Cave<sup>1</sup>, Toru Hatsukade<sup>1,2</sup>, David N. Abram<sup>1</sup>,  
Kendra P. Kuhl<sup>1</sup>, Christopher Hahn<sup>1,2</sup>, Jens K. Nørskov<sup>1,2</sup>, and Thomas F. Jaramillo<sup>1,2\*</sup>

<sup>1</sup> Department of Chemical Engineering, Stanford University, Stanford, California 94305, USA

<sup>2</sup> SUNCAT Center for Interface Science and Catalysis, SLAC National Accelerator Laboratory,  
Menlo Park, California 94025

\*e-mail: jaramillo@stanford.edu

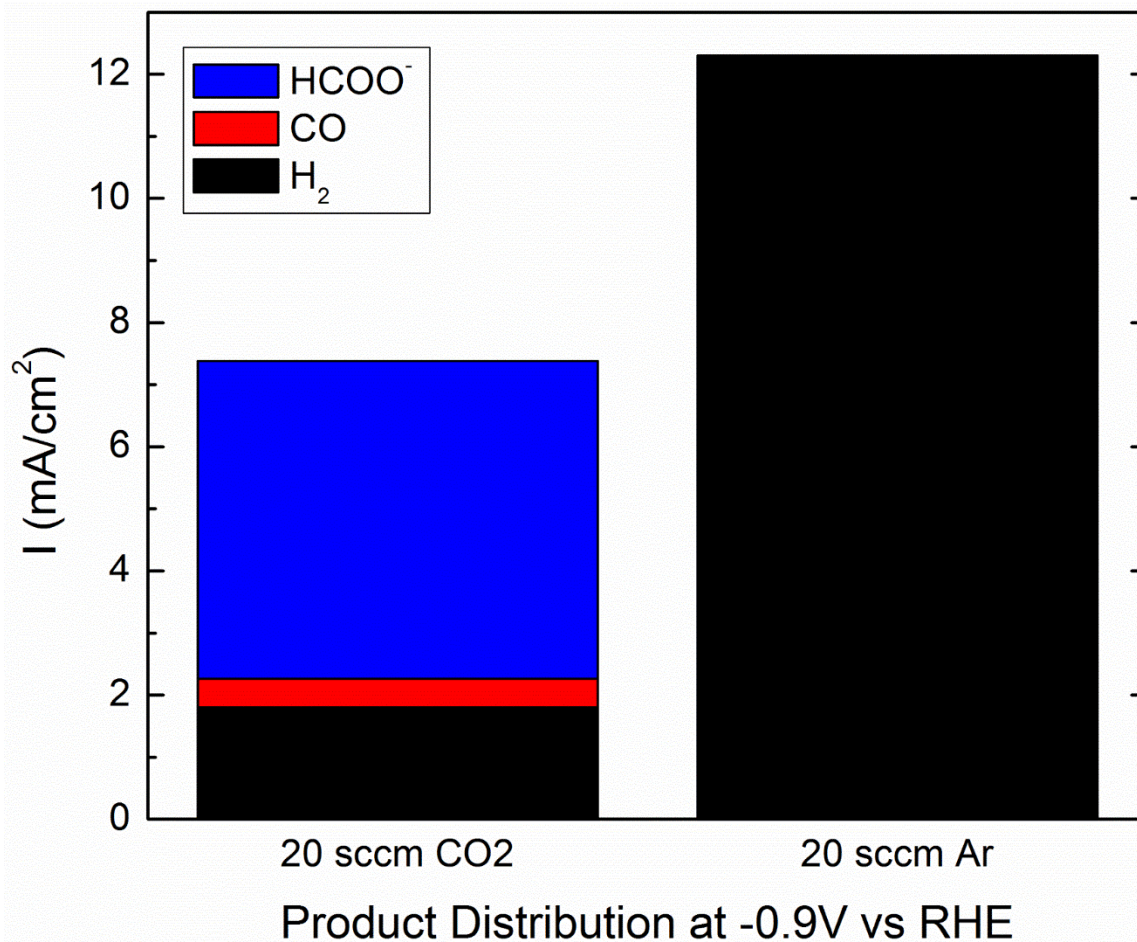


**Figure S1.**  $\text{HCO}_3^-$  was investigated as a potential source for  $\text{HCOO}^-$  and  $\text{CO}$  production on Sn. While both products were observed when 20 sccm  $\text{CO}_2$  was flowed through the electrochemical cell, only  $\text{H}_2$  was observed when the gas flow was replaced with Ar and the only source of carbon was  $\text{HCO}_3^-$ . This indicates that  $\text{CO}_2$ , and not  $\text{HCO}_3^-$ , is the primary reactant for the production of  $\text{CO}$  and  $\text{HCOO}^-$  on Sn.

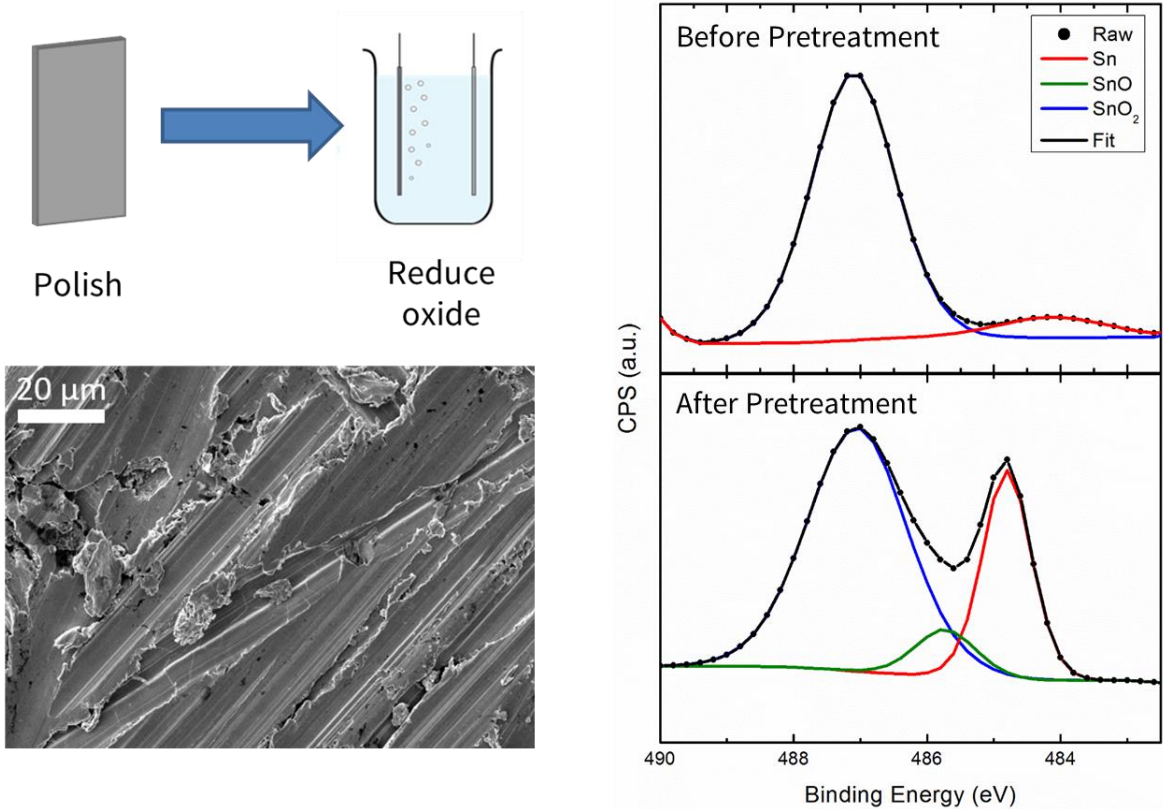


**Figure S2.** The pretreatment used to clean the Sn electrodes consists of a mechanical polish and an electrochemical polish. The SEM image on the left is of the Sn electrode after the polishing steps. The XPS spectra shows that the electrochemical polish reduces the oxide on the surface, leaving only a native oxide.

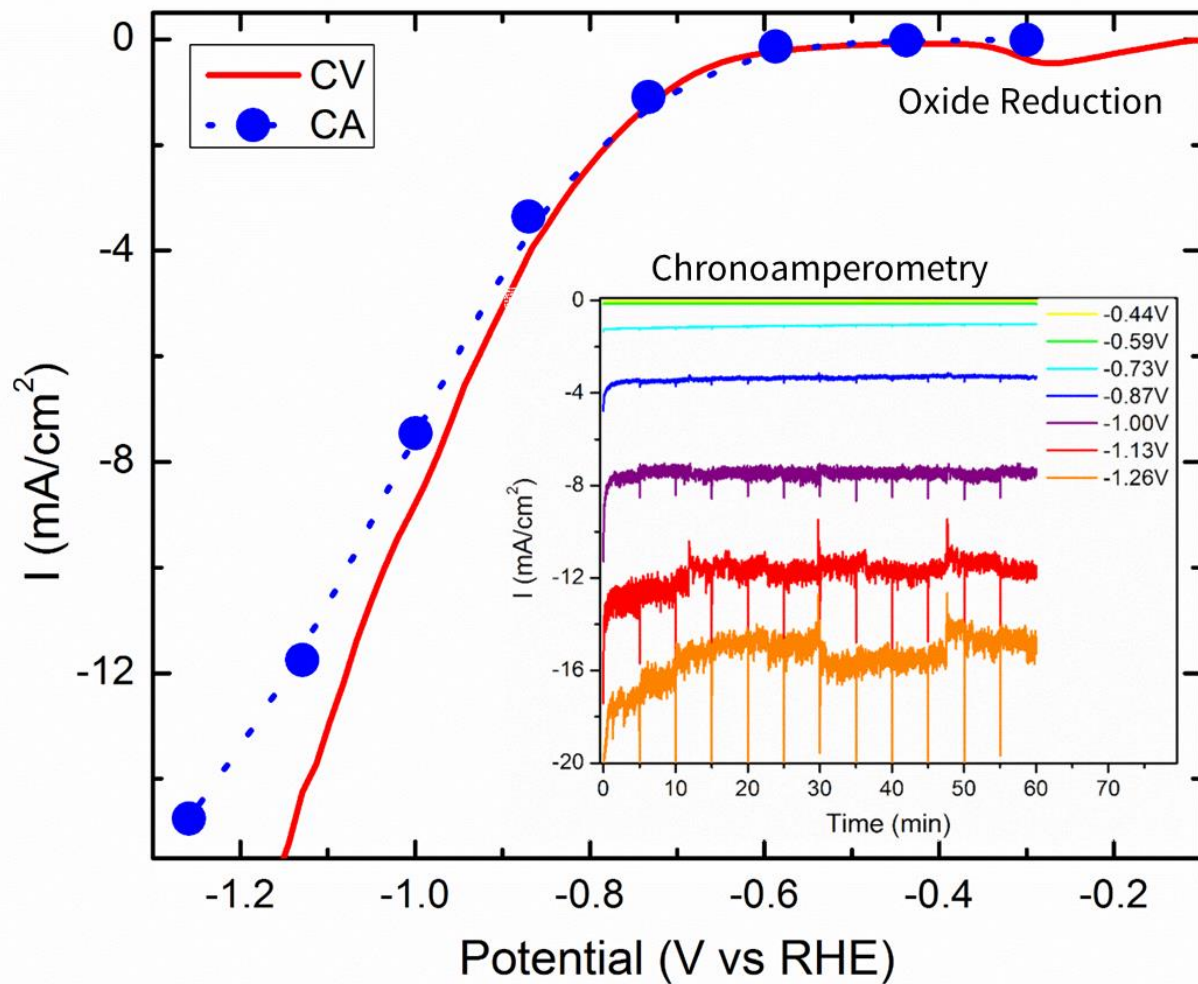


**Figure S3.** Chronoamperometry (CA) and cyclic voltammetry (CV) were used to characterize the CO<sub>2</sub>RR on Sn electrodes. The native oxide layer was reduced on the Sn electrode during the first cathodic CV sweep. The hysteresis between the CA and CV data comes from the time spent at each potential: the CV sweeps at 50 mV/s, while the CA remains at a single potential for one hour.

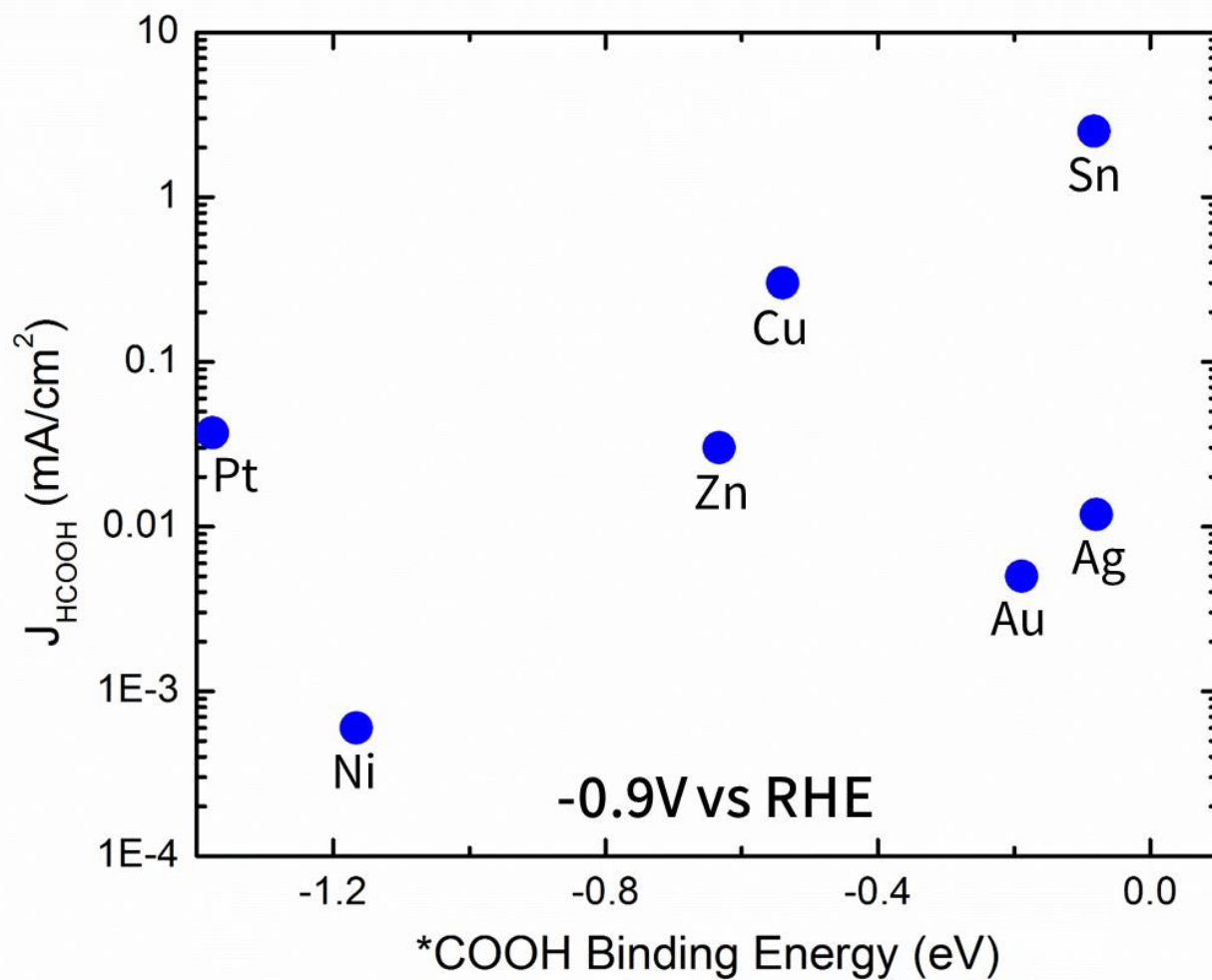


**Figure S4.** HCOO<sup>-</sup> production at -0.9 V vs RHE vs. \*COOH binding energies for select metals. No trend is observed, suggesting that a carbon-bound intermediate is not the primary intermediate for CO<sub>2</sub>RR to HCOO<sup>-</sup>.

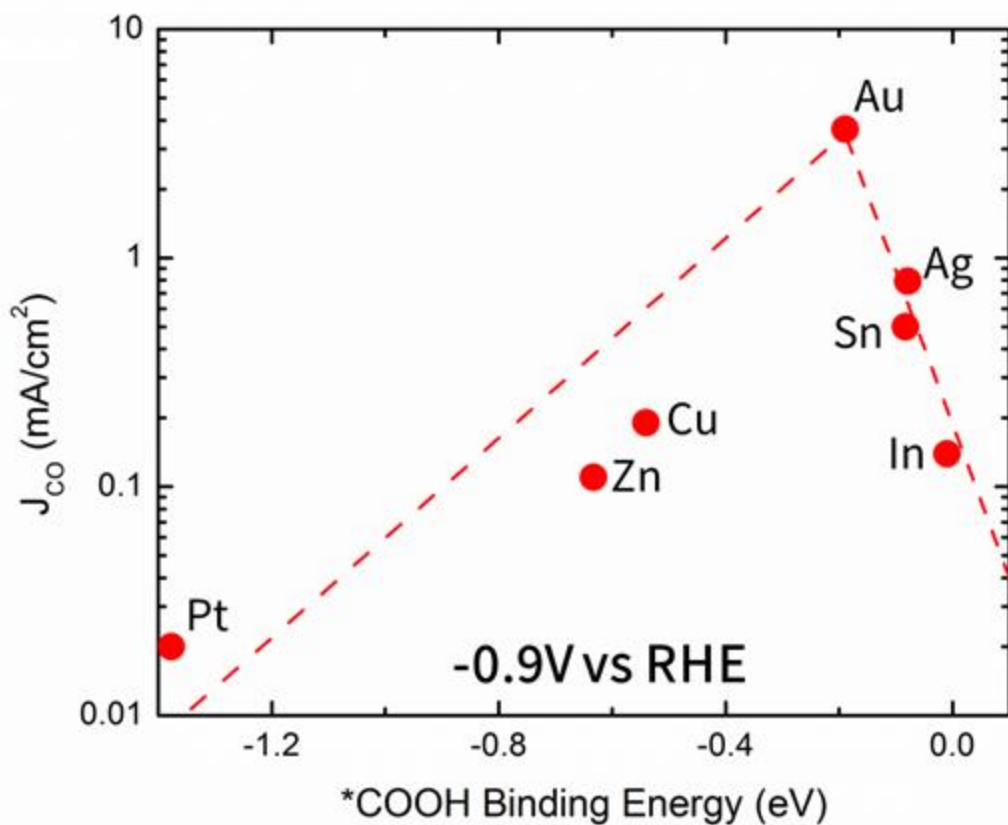


**Figure S5.** This volcano plot is a modified version of Figure 2 that includes In. Electrochemical experiments and \*COOH binding energy calculations were performed for polycrystalline In foil in a manner consistent with the other metals in the plot. By using \*COOH binding energies as a descriptor for CO partial current densities at -0.9 V vs. RHE, a volcano relationship can be established, suggesting that \*COOH binding energy is a key descriptor for CO<sub>2</sub> reduction to CO.

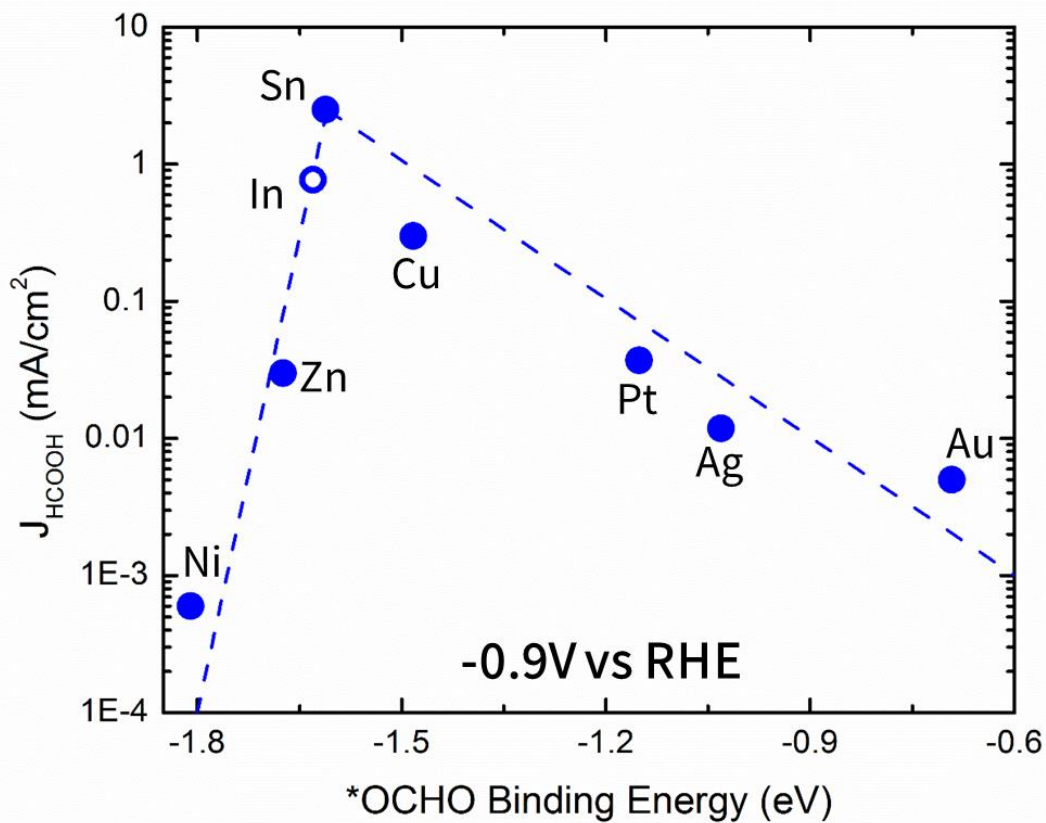


**Figure S6.** This volcano plot is a modified version of Figure 3 that includes In. Electrochemical experiments were performed for polycrystalline In foil in a manner consistent with the other metals in the plot. The \*OCHO binding energy value for In was approximated using scaling relations. By using \*OCHO binding energy as a descriptor for  $\text{HCOO}^-$  partial current density at -0.9 V vs. RHE, a volcano relationship can be established, suggesting that \*OCHO binding energy is a key descriptor for  $\text{CO}_2$  reduction to  $\text{HCOO}^-$ .

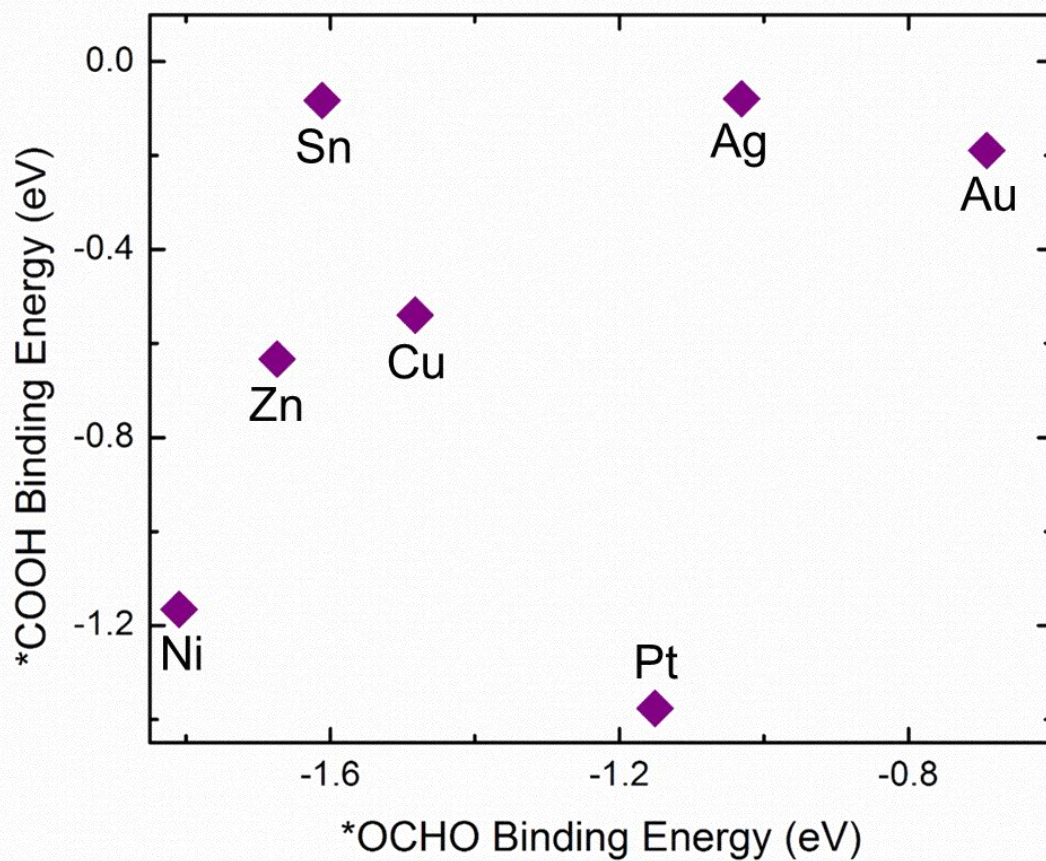


**Figure S7.** \*OCHO binding energies vs. \*COOH binding energies for select metals. No trend is observed, suggesting that there is no scaling relation between \*OCHO and \*COOH binding energies. This indicates that both carbon and oxygen affinities are important for understanding selectivity for CO<sub>2</sub>RR.